

We are IntechOpen, the world's leading publisher of Open Access books Built by scientists, for scientists

4,800

Open access books available

122,000

International authors and editors

135M

Downloads

Our authors are among the

154

Countries delivered to

TOP 1%

most cited scientists

12.2%

Contributors from top 500 universities



WEB OF SCIENCE™

Selection of our books indexed in the Book Citation Index
in Web of Science™ Core Collection (BKCI)

Interested in publishing with us?
Contact book.department@intechopen.com

Numbers displayed above are based on latest data collected.
For more information visit www.intechopen.com



Nonlinear Giant Magnetostrictive Actuator and Its Application in Active Control

Lihua Yang, Haipeng Zhang, Hailong Jiang, Shuyong Liu, Haiping Wu, Haifeng Li and Ehsan Noroozinejad Farsangi

Abstract

The giant magnetostrictive actuator has great use in vibration control, but the linear model cannot fully describe its dynamic characteristics. In this chapter, based on the domain wall theory and piezomagnetic theory, a hysteresis nonlinear model is established to fully describe the actuator dynamic characteristics. In combination with the regularisation method, a sliding mode controller has been designed, and the giant magnetostrictive actuator is also studied in the application of active control. Experimental results show that the hysteresis nonlinear model proposed in the chapter can fully describe the actuator's dynamic characteristics in a wider frequency band and the active control also has a much better isolation effect than the passive vibration; it can significantly attenuate the external incentives.

Keywords: giant magnetostrictive actuator, hysteresis nonlinearity, sliding mode control, active control

1. Introduction

Passive vibration isolation has been widely used as an effective isolation method; it can significantly reduce the vibration transmission between mechanical equipment and the base, while the isolation effect is limited in the micro-vibration and low frequencies. Therefore, the active control has been a focus of research at home and abroad [1–4]. With the development of smart materials, intelligent actuators manufactured by those materials including the magneto-rheological actuator, shape memory alloy actuator, giant magnetostrictive actuator (GMA), and others. These actuators have played a huge role in promoting the active control as the executing agency [5, 6].

With the advantages of high-positioning accuracy, fast response, and wide frequency band, among others, the GMA has a wide variety of applications in fields including vibration control and precision positioning [7–10]. Many scholars have studied the linear modelling method of GMA, which is only suitable for describing low-frequency dynamic characteristics [11, 12]. However, the hysteresis nonlinear model based on the domain walls theory can more clearly reveal the coupling relationship among the magnetization process, the stress magnetic machine effect, and stretching amount, and it can more fully describe the GMA's dynamic characteristics on a wide frequency band [13], which is suitable for the active control

actuator. Zhang established the GMA dynamics equations and studied the active control on the basis of the proportional-integral-derivative (PID) algorithm, the results showed that the GMA has some damping effect, but the system's adaptive capacity is a little weak [14]. Francesco calculated the actuator's amplitude-frequency curve and studied the active control in a single freedom degree vibration isolation system. The simulations showed the GMA can significantly reduce the force transmitted to the base [15]. Wang designed a magnetostrictive actuator rod and analysed the system structure vibration on the basis of the linear-quadratic regulator (LQR) algorithm, the results showed the GMA can effectively reduce the structure response of acceleration and displacement [16]. However, these studies mainly focus on the linear actuator model; the isolation frequency band is narrow relatively. Therefore, the application of the GMA hysteresis nonlinear model is urgently needed in the active control.

Currently, some of the more commonly active control strategies are the PID control [17], robust control [18], fuzzy control [19], optimal control [20], adaptive control [21], and sliding mode control [22]. In particular, the sliding mode control has no effect on system parameter perturbation and external disturbance when the system is in sliding mode, so it has much better robustness [23], which is more suitable for the active vibration control algorithm.

Based on the domain wall theory [24], this chapter studied the GMA broadband hysteresis nonlinear model and applied it to the active control of the vibration isolation system. By optimising the design of the hysteresis nonlinear model, the actuator linearity is much better than the linear model on a wider frequency band. The results showed that the GMA hysteresis nonlinear model on a wider frequency band can more fully describe its dynamic characteristics. Compared with passive vibration isolation, the active control has a better isolation effect and wider frequency band isolation, and the sliding mode control strategy also has stronger robustness.

2. Hysteresis nonlinear magnetostrictive actuator model

2.1 Magnetostrictive actuator model

The GMA structure is shown in **Figure 1**. It is mainly made of the push rod, preload spring, magnetostrictive rod, drive coil, and bias coil, where the preload mechanism is comprised of the preload spring, push rod, and preload screw. The polarised magnetic field of the bias coil can make the magnetostrictive rod deform in a linear manner and can prevent the multiplier phenomenon from affecting system control precision. When an alternating current is passed through the drive coil, the magnetostrictive rod can also generate an alternating magnetic field, which causes a dynamic redistribution of magnetic domains in the magnetostrictive rod. Then the telescopic length can be obtained microscopically to promote a displacement and thrust the output push rod, which achieves energy conversion by transferring electromagnetic energy into mechanical energy.

Based on the Jiles-Atherton theory [25], many researchers explored the GMA characteristics of the nonlinear hysteresis model, and the structure optimisation and parameter configuration can make the theoretical calculations accurately match with experiments in a higher linearity. Generally, the GMA motion can be equivalent to a single freedom degree model, shown in **Figure 2**. Based on the magnetic domain theory and piezomagnetic theory [26–28], the partial differential equations of the magnetisation process are established. Then the GMA dynamics equation is also deduced with the specific equations as follows:

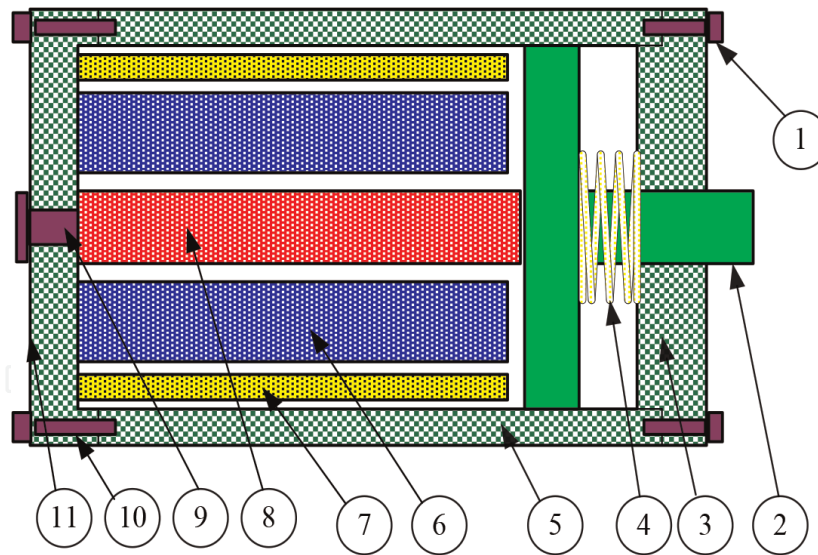


Figure 1.
 The GMA structure. (1) The top cover screw, (2) the output push rod, (3) the top cover, (4) the preload spring, (5) the jacket, (6) the drive coil, (7) the bias coil, (8) the magnetostrictive rod, (9) the preload screw, (10) the bottom cover screws, and (11) the bottom cover.

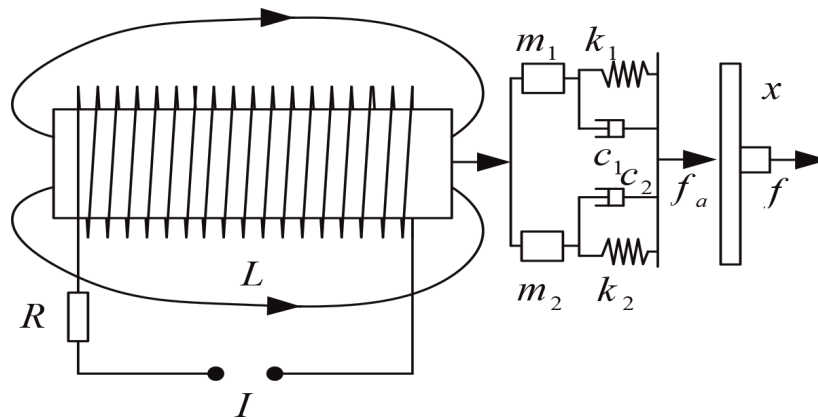


Figure 2.
 The GMA schematic diagram.

$$H_e = H + \alpha M + H_\sigma = H + \alpha M + 3 \frac{\tilde{\sigma}}{2\mu_0} \left(\frac{d\lambda}{dM} \right)_\sigma \quad (1)$$

$$M_{an} = M_s [\coth(H_e/a) + a/H_e] \quad (2)$$

$$\frac{dM_{irr}}{dH} = \frac{M_{an} - M_{irr}}{\delta k - \tilde{\alpha}(M_{an} - M_{irr})} \quad (3)$$

$$M_{rev} = c(M_{an} - M_{irr}) \quad (4)$$

$$M = M_{irr} + M_{rev} \quad (5)$$

$$\lambda = \frac{3}{2} \frac{\lambda_s}{M_s^2} M^2 \quad (6)$$

$$x_{(s)} = \frac{1}{(m_1 + m_2)s^2 + (c_1 + c_2)s + (k_1 + k_2)} \frac{A}{S^H} \lambda \quad (7)$$

$$f = \frac{m_2 s^2 + c_2 s + k_2}{(m_1 + m_2)s^2 + (c_1 + c_2)s + (k_1 + k_2)} \frac{A}{S^H} \lambda \quad (8)$$

where H_e is the effective magnetic field strength, H is the sum of the drive magnetic field $H_d = nI$ (n is the number of turns per unit coil length, I is the drive

current) and bias magnetic field H_b , λ_s is the saturation magnetostrictive coefficient, $\tilde{\sigma} = \sigma_0 + \sigma$ is the external stress (σ_0 is the preload), μ_0 is the vacuum permeability, M_s is the saturation magnetisation, λ is the axial magnetostriction strain, a is the shape factor of non-hysteresis magnetisation, k is the irreversible loss coefficient, α is the molecular field parameter of interacting magnetic torque, $\tilde{\alpha} = \alpha + 9\lambda_s\sigma_0/2\mu_0M_s^2$ is the integrated magnetic domain coefficient, c is the reversible factor, the parameter $\delta \equiv +1$ when $dH > 0$ and parameter $\delta \equiv -1$ when $dH < 0$, M_{an} is the non-hysteresis magnetisation, M_{irr} is the irreversible magnetisation, M_{rev} is reversible magnetisation, and M is the total magnetisation. C , ρ , L , A , and S^H are, respectively, the damping, density, length and cross-sectional area, and axial compliance coefficient of the magnetostrictive rod; $m_1 = \rho LA/3$, $c_1 = cA/L$, and $k_1 = A/S^H L$ are, respectively, the equivalent mass, damping, and stiffness coefficient of the magnetostrictive rod; m_2 , c_2 , and k_2 are, respectively, the equivalent mass, damping, and stiffness coefficient of the end load; and s is the Laplace transform operator.

2.2 Magnetostrictive actuator model for wide frequency range

When the driving frequency is low, temperature and eddy current can be ignored on the actuator linearity. However, to fully describe the actuator dynamic characteristics on a wide frequency range, it is necessary to consider the hysteresis loss, eddy current losses, additional loss, and stress changes. In this case, magnetisation intensity M can be expressed as follows:

$$\frac{dM}{dt} = \frac{\partial M}{\partial H} \frac{dH}{dt} + \frac{\partial M}{\partial \sigma} \frac{d\tilde{\sigma}}{dt} \quad (9)$$

where magnetisation change rate is made up of differential susceptibility $\partial M/\partial H$, the magnetic field change rate $\partial H/\partial t$, magnetisation stress change rate $\partial M/\partial \sigma$, and stress change rate $\partial \tilde{\sigma}/\partial t$. The key is to solve for $\partial M/\partial H$ and $\partial \tilde{\sigma}/\partial t$. By Eqs. (2)–(5), the differential susceptibility can be expressed as such:

$$\frac{\partial M}{\partial H} = (1 - c) \frac{M_{an} - M_{irr}}{\delta k - \tilde{\alpha}(M_{an} - M_{irr})} + c \frac{\partial M_{an}}{\partial H} \quad (10)$$

According to magneto-mechanical coupling model [16], the magnetisation stress change rate can be determined by Eq. (11):

$$\frac{\partial M}{\partial \sigma} = \frac{S^H \sigma}{\xi} (M_{an} - M) + c \frac{\partial M_{an}}{\partial \sigma} \quad (11)$$

where ξ is the energy coupling parameters of per unit volume and other parameters are the same as above. Substituting Eqs. (10) and (11) into Eq. (9), the magnetisation change rate can be obtained:

$$\begin{aligned} \frac{dM}{dt} = & \left((1 - c) \frac{M_{an} - M_{irr}}{\delta k - \tilde{\alpha}(M_{an} - M_{irr})} + c \frac{\partial M_{an}}{\partial H} \right) \frac{dH}{dt} \\ & + \left(\frac{S^H \sigma}{\xi} (M_{an} - M) + c \frac{\partial M_{an}}{\partial \sigma} \right) \frac{d\tilde{\sigma}}{dt} \end{aligned} \quad (12)$$

In summary, Eqs. (1)–(12) constitute the hysteresis nonlinear model of the giant magnetostrictive actuator, which can describe the displacement and force

output on a wide frequency range, and then the output displacement and force can be calculated by the input current.

3. Giant magnetostrictive actuator experiment

The experiments mainly include the giant magnetostrictive actuator, NI host controller, capture cards and displays, LabVIEW software, FN15150 power amplifier, MEL laser displacement sensor, and CHINT current transformer. NI equipment and software are used to capture and display the current and displacement signal, the amplifier amplifies NI weak signals to drive actuators, and the laser displacement sensor is used to accurately measure the actuator displacement. The GMA experiment setup is shown in **Figure 3**. This experiment studies the hysteresis nonlinear model displacement responses to the preload and the bias magnetic field intensity, as shown in **Figures 4** and 5. By optimising the actuator preload and bias magnetic field, the GMA can eliminate the doubling phenomenon and work perfectly within a linear range, which can enhance the actuator output linearity.

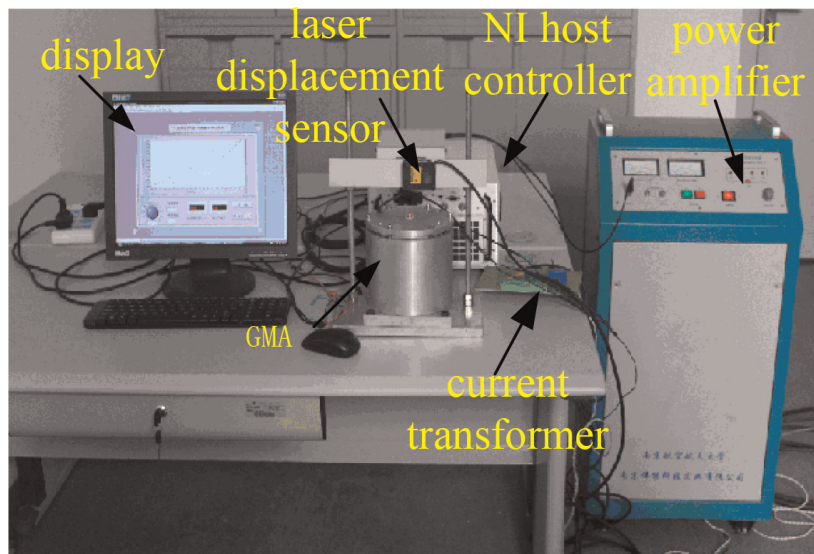


Figure 3.
The giant magnetostrictive actuator experiment.

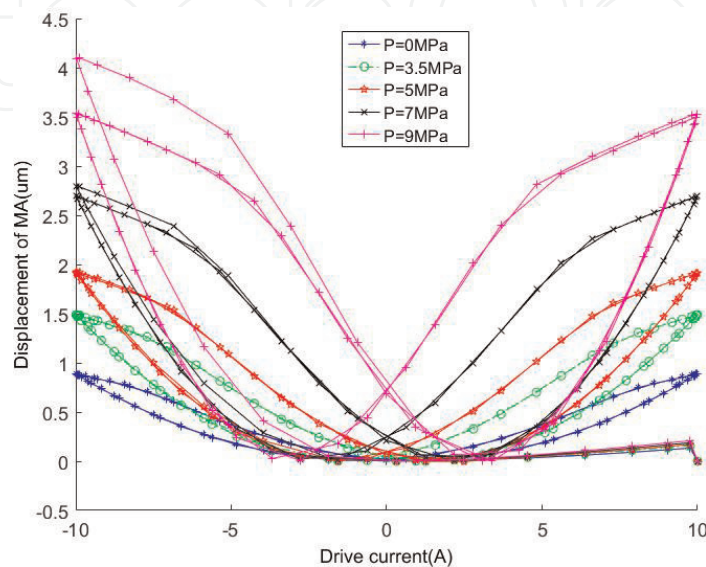


Figure 4.
Curves of displacement changes with the preload.

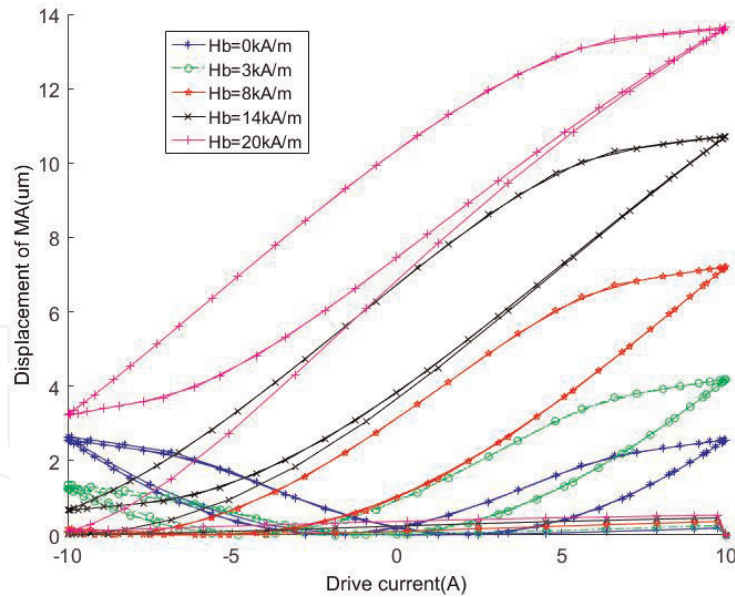


Figure 5.
Curves of displacement changes with the bias magnetic field intensity.

Figure 4 shows that the actuator displacement increases with the preload, but when the preload is greater than 7 MPa, experimental curves began to appear asymmetrical, so the preload cannot be greater than 7 MPa. **Figure 5** shows that without the paranoid magnetic field, actuator output is butterfly-shaped with a strong nonlinearity, but when the paranoid magnetic field increases, the output linearity also gradually increases. Finally, $\sigma_0 = 6.7MPa$ and $H_b = 14kA/m$ are selected in the study which can give the actuators better linearity.

4. Application for GMA in active control

4.1 Active control model of vibration isolation system

The active control model of the vibration isolation system is shown in **Figure 6**, where M_1 , K_1 , C_1 , M_2 , K_2 , and C_2 are, respectively, the mass, stiffness, and damping of the upper isolated equipment and the middle vibration isolation platform. x , y , \dot{x} , \dot{y} , \ddot{x} , and \ddot{y} are, respectively, displacement, velocity, and acceleration as above. f is the active control force of the GMA, and p is the external disturbance. The dynamics equations of the isolation system can be expressed as Eq. (13):

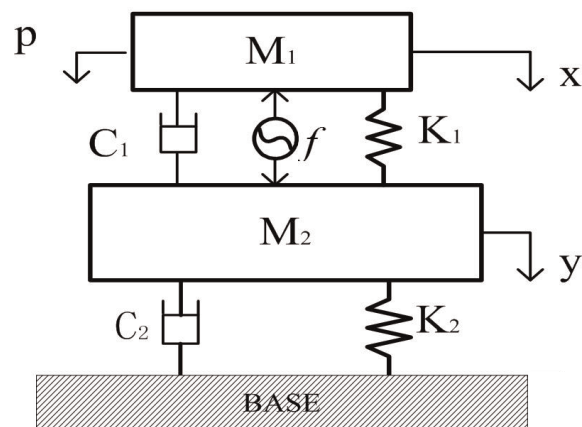


Figure 6.
Active control model of vibration isolation system.

$$\begin{cases} M_1\ddot{x} + C_1(\dot{x} - \dot{y}) + K_1(x - y) = p - f \\ M_2\ddot{y} + C_2\dot{y} + K_2y + C_1(\dot{y} - \dot{x}) + K_1(y - x) = f \end{cases} \quad (13)$$

Take $X = [x, y, \dot{x}, \dot{y}]^T$ as state variables and the middle platform displacement $Y = y$ as system output. Thus, the state space can be obtained using Eq. (14):

$$\begin{cases} \dot{X}(t) = AX(t) + Bu(t) + B_1w(t) \\ Y(t) = CX(t) \end{cases} \quad (14)$$

where $A = \begin{bmatrix} 0 & 0 & 1 & 0 \\ 0 & 0 & 0 & 1 \\ -K_1/M_1 & K_1/M_1 & -C_1/M_1 & C_1/M_1 \\ K_1/M_2 & -(K_1 + K_2)/M_2 & C_1/M_2 & -(C_1 + C_2)/M_2 \end{bmatrix}$,

$B = \begin{bmatrix} 0 \\ 0 \\ -1/M_1 \\ 1/M_2 \end{bmatrix}$, $B_1 = \begin{bmatrix} 0 \\ 0 \\ 1/M_1 \\ 0 \end{bmatrix}$, $C = [0 \ 1 \ 0 \ 0]$, $u = [f]$, $w = [p]$, and $Y = [y]$. Let

$U = u + B^{-1}B_1w$. Eq. (14) can be further expressed as follows:

$$\begin{aligned} \dot{X}(t) &= AX(t) + Bu(t) + B_1w(t) \\ &= AX(t) + BU(t) \end{aligned} \quad (15)$$

4.2 Sliding mode control design

Based on full state feedback, the sliding mode can make the system reach the sliding mode surface and achieve sliding mode movement in a jump way. Therefore, it is essential for dynamic characteristics to rationally design the sliding mode surface, assuming the system switching function as Eq. (4) [29, 30].

$$S(t) = \Theta X \quad (16)$$

where S is the switching function, Θ is 1×4 dimension switching matrix, and $X = [x, y, \dot{x}, \dot{y}]^T$ are the state variables. The non-singular state transition matrix $\Gamma \in R^{4 \times 4}$ is taken to regulate Eq. (16), and the coordinate transformation is the following:

$$Z(t) = \Gamma X(t) \quad (17)$$

where $\Gamma = \begin{bmatrix} I_3 & -\tilde{B}_1\tilde{B}_2 \\ 0 & I_1 \end{bmatrix}$, $B = \begin{bmatrix} \tilde{B}_1 \\ \tilde{B}_2 \end{bmatrix}$, $\tilde{B}_1 \in R^{3 \times 1}$, and $\tilde{B}_2 \in R^{1 \times 1}$; substituting

Eq. (17) into Eqs. (15) and (16), it gets the system canonical form and the switching surface as Eq. (18):

$$\begin{aligned} \dot{Z}(t) &= \bar{A}Z(t) + \bar{B}U(t) \\ S(t) &= \bar{\Theta}Z \end{aligned} \quad (18)$$

where $\bar{A} = \Gamma A \Gamma^{-1}$, $\bar{B} = \begin{bmatrix} 0 & \tilde{B}_2^T \end{bmatrix}^T$, and $\bar{\Theta} = \Theta \Gamma^{-1}$; let $Z(t) = \begin{bmatrix} Z_1(t) \\ Z_2(t) \end{bmatrix}$,

$\bar{A} = \begin{bmatrix} \bar{A}_{11} & \bar{A}_{12} \\ \bar{A}_{21} & \bar{A}_{22} \end{bmatrix}$, and $\bar{\Theta} = \begin{bmatrix} \bar{\Theta}_1 \\ \bar{\Theta}_2 \end{bmatrix}^T$, where $Z_1(t) \in R^{3 \times 1}$, $Z_2(t) \in R^{1 \times 1}$, $\bar{A}_{11} \in R^{3 \times 3}$, $\bar{A}_{12} \in R^{3 \times 1}$, $\bar{A}_{21} \in R^{1 \times 3}$, and $\bar{A}_{22} \in R^{1 \times 1}$; then Eq. (18) can be decomposed as Eq. (19):

$$\begin{aligned}\dot{Z}_1(t) &= \bar{A}_{11}Z_1(t) + \bar{A}_{12}Z_2(t) \\ S &= \bar{\Theta}_1Z_1(t) + \bar{\Theta}_2Z_2(t)\end{aligned}\quad (19)$$

Let $S = 0$ and $\bar{\Theta}_2 = I_1$; in Eq. (19), it gets:

$$\begin{aligned}Z_2(t) &= -\bar{\Theta}_1Z_1(t) \\ \dot{Z}_1(t) &= (\bar{A}_{11} - \bar{A}_{12}\bar{\Theta}_1)Z_1(t)\end{aligned}\quad (20)$$

where the matrix $\bar{\Theta}_1$ can be designed by the optimal control method or pole assignment method, and then the sliding surface $S(t)$ can also be determined. Finally, the saturation function of exponential reaching law is used as Eq. (21):

$$\dot{S}(t) = -\beta S(t) - \xi \text{sat}(S(t)) \quad \xi > 0, \beta > 0 \quad (21)$$

where $\alpha > 0$ and $1 > \beta > 0$; with the combination of Eqs. (15), (16), and (21), it can get active control force as Eq. (22) by ignoring the external disturbances:

$$f = -(\Theta B)^{-1}[\Theta AX(t) + \beta S(t) + \xi \text{sat}(S(t))]\quad (22)$$

5. Experimental research

In this chapter, compared with passive vibration isolation, the active control experiment is studied to analyse the isolation effect on a double-layer vibration isolation system. The external disturbance is the force of shaker JZK-40, the hardware control system is designed by LabVIEW real time, and the isolation system experiment setup is shown in **Figure 7**.

When the external stimulus is applied to the system, the controllers can capture the acceleration signal of the upper and middle layers; then the signal is conveyed to a controller by an A/D converter. At the same time, D/A signals are given out by NI control calculations, passing through amplifier YE2706A, and the output finally is transmitted to GMA for carrying out the active control. The vibration isolation system control block diagram is shown in **Figure 8**.

In low frequencies, taking the middle platform displacement as the evaluation index, the isolation effect is compared between passive vibration isolation and active control. Experimental parameters are as follows:

$$\begin{aligned}n &= 1200, H_b = 10kA/m, a = 7102A/m, \tilde{\alpha} = -0.01, M_s = 7.65 \times 10^5 A/m, \\ \lambda_s &= 1.005 \times 10^{-6}, k = 3283A/m, b = 0.18, S^H = 1.3 \times 10^{-11}, d = 1.0 \times 10^{-8}m^2/N, \\ \xi &= 7600Pa, C = 3000kNs/m^2, \rho = 9250kg/m^3, L = 8.6 \times 10^{-4}m, A = 78.5 \times 10^{-6}m^2, \\ M_1 &= 155.42kg, C_1 = 302.7Ns/m, K_1 = 57016.2N/m, M_2 = 22.5kg, C_2 = 290.544Ns/m, \\ \text{and } K_2 &= 190000N/m.\end{aligned}\quad (23)$$

The system's natural frequency ($f_1 = 2.8Hz, f_2 = 15.6Hz$) can be calculated according to the above parameters, and the external disturbances were taken as single, multi-frequency, and random signals. The experimental results are in **Figures 9–13** and in **Table 1**.

Figures 9–12 show that active control can effectively suppress the vibration generated by external incentives with a significant isolation effect and speed response. **Table 1** shows that, compared with the passive vibration isolation, the

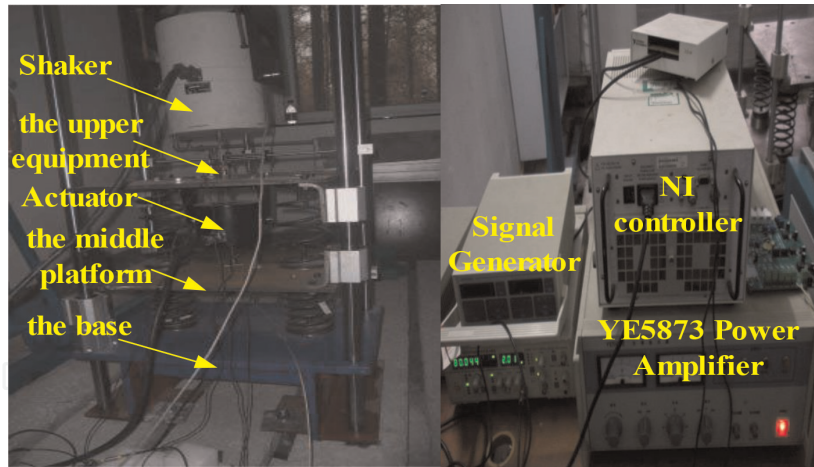


Figure 7.
 The isolation system experiment setup.

active control makes the middle raft displacement decrease by 81.08, 78.21, 81.13, and 55.34% in a single frequency, multi-frequency, and random excitation, respectively. Therefore, the active control has obvious advantages and a good isolation effect.

Figure 13 shows that the natural frequencies corresponding to the two peaks of the passive isolation system are fully consistent with the calculations. Moreover, the active control can change the system mode to eliminate the first- and second-order formants to achieve the purpose of isolation. It also shows the active control is poor when the excitation frequency is less than 2 Hz, and then the isolation effect increases with escalating excitation frequency. However, there are always cross-points between active control and passive vibration isolation in the amplitude-frequency curve, which also shows the active control is more suitable for low- and middle-frequency vibration control. It can compensate for the lack of passive vibration isolation and effectively inhibit the transmission of vibration isolation and broaden isolation frequency band, all of which are of great significance for the study of active vibration control in engineering applications.

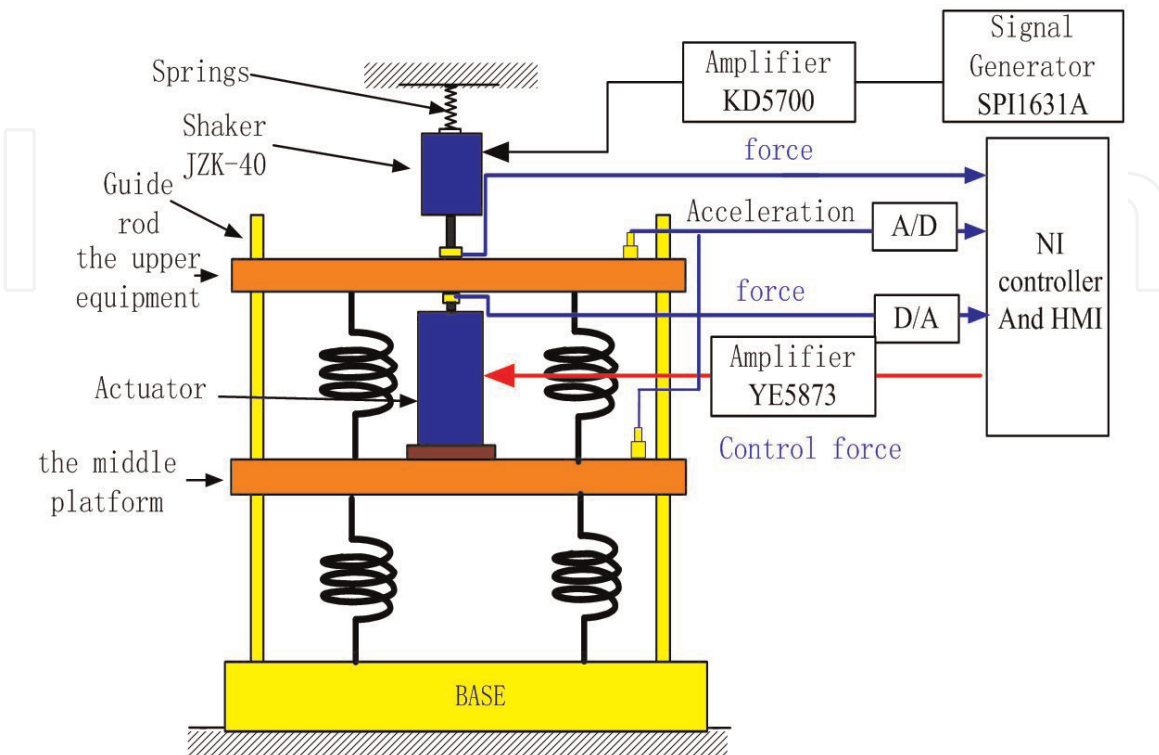


Figure 8.
 Vibration isolation system control block diagram.

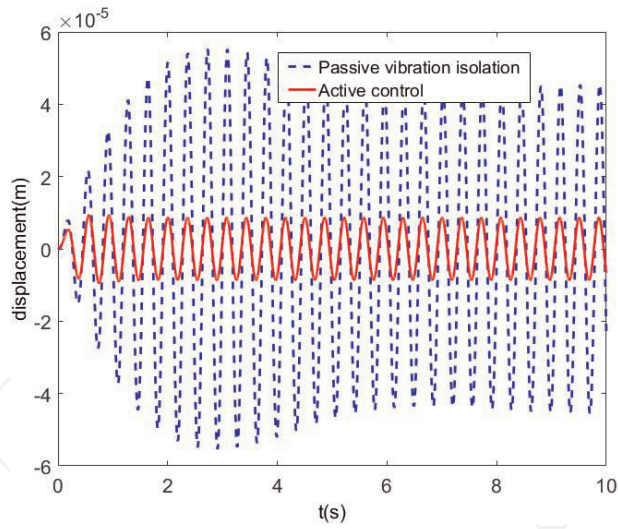


Figure 9.
The time history of middle-layer displacement with f_1 excitation.

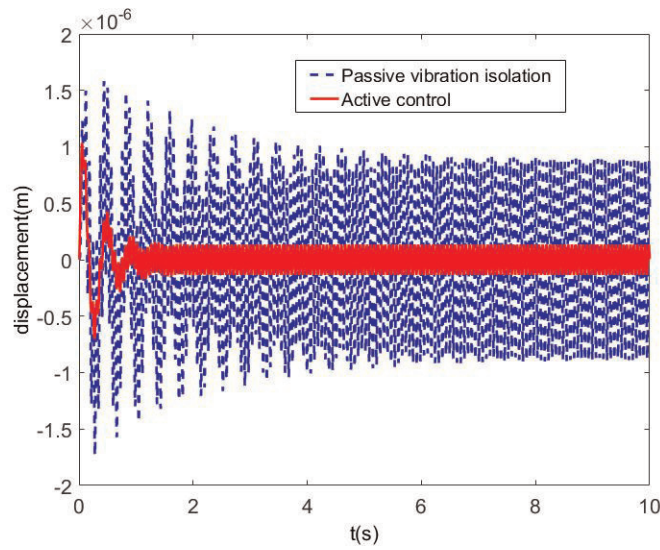


Figure 10.
The time history of middle-layer displacement with f_2 excitation.

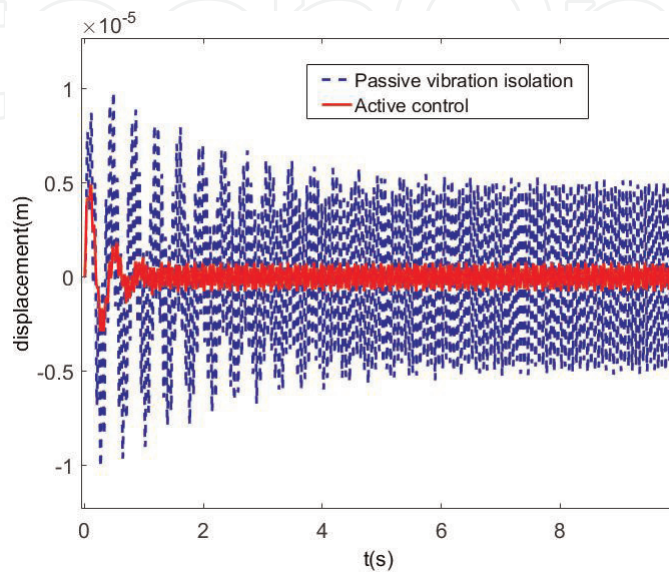


Figure 11.
The time history of middle-layer displacement with $\sqrt{2}f_1 + \sqrt{2}f_2 + 50$ excitation.

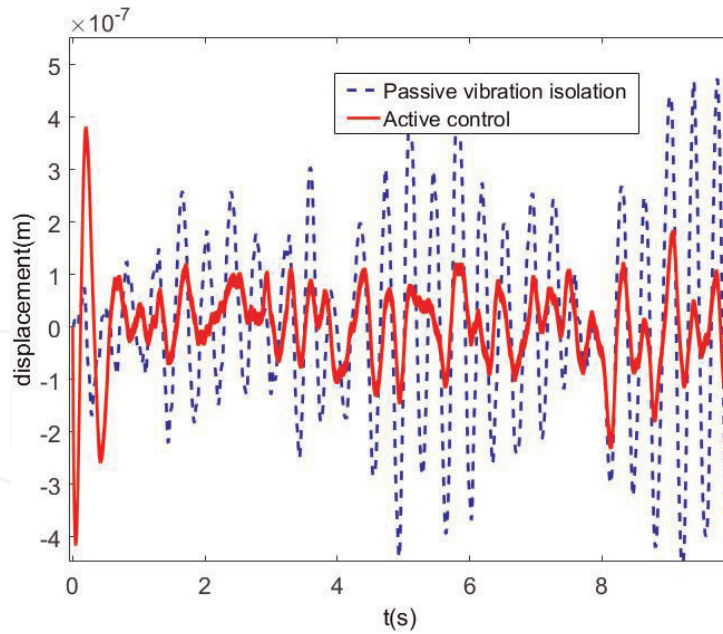


Figure 12.
 The time history of middle-layer displacement with random excitation.

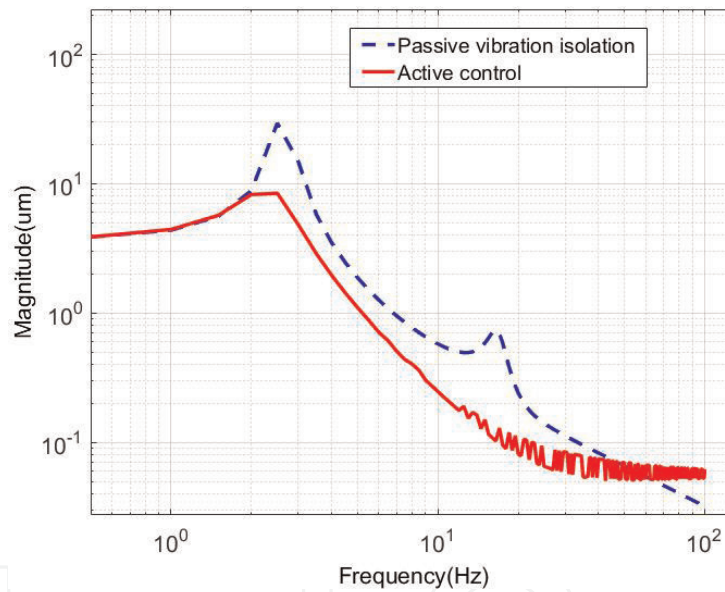


Figure 13.
 The amplitude-frequency curves of middle-layer displacement.

	The middle-layer displacement RMS			
	f_1	f_2	$\sqrt{2}f_1 + \sqrt{2}f_2 + 50$	Random
Passive vibration isolation	32.1970	0.6576	3.7067	0.1892
Active control	6.0899	0.1432	0.6996	0.0845

Table 1.
 The middle-layer displacement RMS with excitations.

6. Conclusions

In this study, GMA linear model cannot fully describe the dynamic behaviour. Based on the magnetic domain theory, piezomagnetic theory, and with the consideration of the magnetic hysteresis, eddy current, and alternating stress, the GMA

hysteresis nonlinear model is established, which can describe the actuator dynamic characteristics in a broadband segment. The GMA is then used in active control with the sliding mode control theory. The experimental results show that the hysteresis nonlinear model can fully describe the actuator dynamic characteristics in a broadband segment; the active control is better than passive isolation in single, multi-frequency, and random excitation; and it can effectively broaden the isolation frequency band and improve the response speed and suppress vibration transmission. But it also has some isolation range, which means the effect will deteriorate beyond the effective frequency isolation band.

Acknowledgements

This work was supported by the State Key Laboratory of Ocean Engineering (Shanghai Jiao Tong University) (Grant no. 1714) project ZR2019QEE031 supported by Shandong Provincial Natural Science Foundation and the National Natural Science Foundation of China (51579242, 51509253).

Conflict of interest

The authors declare that there are no conflicts of interest regarding the publication of this chapter.

Author details

Lihua Yang^{1*}, Haipeng Zhang¹, Hailong Jiang¹, Shuyong Liu², Haiping Wu¹, Haifeng Li¹ and Ehsan Noroozinejad Farsangi³


¹ Power Control Department, Navy Submarine Academy, Qingdao, P.R. China

² College of Power Engineering, Naval University of Engineering, Wuhan, P.R. China

³ Faculty of Civil Engineering and Surveying, Graduate University of Advanced Technology, Iran

*Address all correspondence to: dreamfly4@163.com

IntechOpen

© 2019 The Author(s). Licensee IntechOpen. This chapter is distributed under the terms of the Creative Commons Attribution License (<http://creativecommons.org/licenses/by/3.0>), which permits unrestricted use, distribution, and reproduction in any medium, provided the original work is properly cited. 

References

- [1] Gao HW, Luo J, Jia JY. Modeling and simulation of active control of two-layer vibration isolation system. *Mechanical Science and Technology*. 2005;**24**(11): 1340-1344
- [2] Yang TJ, Gu Z, Liu Z. Experimental research on active control of coupled vibration for a two-stage isolation system. *Journal of Vibration Engineering*. 2003;**16**(2):25-27
- [3] Zhang KG, Du QF. Study on active control of vibration in two-layer isolation system with multiple excitations. *China Mechanical Engineering*. 2006;**17**(2):134-136
- [4] He L, Xu W. Naval vessel machinery mounting technology and its recent advances. *Acta Acustica*. 2013;**38**(2): 128-135
- [5] Wang YF, Cheng W. Modeling and simulation of a mini micro-vibration active control platform for spacecrafts. *Journal of Vibration and Shock*. 2013; **32**(22):140-145
- [6] Quan WF, Mao JQ, Li C. Application of intelligent structure and intelligent control in active vibration control. *Information and Electronic Engineering*. 2004;**2**(3):232-237
- [7] Sathishkumar R, Prasath JS. Terfenol-D: A high power giant magnetostrictive material for submarine mapping. *International Journal of Engineering, Science and Technology*. 2010;**2**(12):7165-7170
- [8] Tao ML, Chen DF, Lu QG. Eddy current losses of giant magnetostrictors: Modeling and experimental analysis. *Journal of Mechanical Engineering*. 2012;**48**(13):146-151
- [9] Hu SF, Zhu SJ. High-precision control of giant magnetostrictive actuator based on CMAC neural network. *Journal of Vibration and Shock*. 2009;**28**(3):68-72
- [10] Lau HY, Liu KP. Feasibility of using GMM based actuators in active control of journal bearing system. In: *Proceedings of the World Congress on Engineering; WCE 2009; Vol. II; 1-3 July 2009; London, UK; 2009*
- [11] Valadkhan S, Morris K, Khajepour A. Review and comparison of hysteresis models for magnetostrictive materials. *Journal of Intelligent Material Systems and Structures*. 2009;**20**(1):131-142
- [12] Jia Z, Wang X, Wang F. Identification method of giant magnetostrictive transducer's dynamic parameters and magnetic parameters. *Chinese Journal of Mechanical Engineering*. 2007;**43**(10):9-13
- [13] Jiles DC, Thoelke JB, Devine MK. Numerical determination of hysteresis parameters for the modeling of magnetic properties using the theory of ferromagnetic hysteresis. *IEEE Transactions on Magnetics*. 1992;**28**(1): 27-35
- [14] Zhang TF, Wang HZ, Sun Y. Simulation on active vibration control. *Journal of Vibration and Shock*. 2006; **25**(1):61-65
- [15] Dezza FC, Cinquemani S. A model of magnetostrictive actuators for active vibration control. In: *Proceedings of 2011 IEEE 5th International Conference on Mechanics of Biomaterials & Tissues Italy; 15 February 2011*
- [16] Wang SL, Ji QB, Dai JB. Study on active vibration control of the structure using giant magnetostrictive actuator. *Noise and Vibration Control*. 2010;**6**:23-26
- [17] Li B, Dong W, Wang X. Design and simulation of an active vibration isolator

- based on pneumatic-electromagnetic hybrid driving. *Journal of Northwestern Polytechnical University*. 2013;**31**(6): 871-877
- [18] Hao HR, Bai HB, Zhang HJ. Robust control of a 6-DOF active-passive vibration isolation platform. *Journal of Vibration and Shock*. 2012;**31**(7):122-127
- [19] He X. Fuzzy logic control of double stage vibration isolation system. *Noise and Vibration Control*. 2010;**2**:38-42
- [20] Gao XK, Shao Q. Semi-active optimal control of intelligent damping double vibration isolation system. *Journal of Vibration and Shock*. 2012; **31**(19):128-133
- [21] Li YN, Zhang F, Lei W. Active vibration control of gear meshing based on online secondary path identification algorithm. *Journal of Vibration and Shock*. 2013;**32**(16):7-12
- [22] Qinlei H, Guangfu M, Jiang Y. Variable structure control with time varying sliding mode and vibration control for flexible satellite. *Control Theory & Applications*. 2009;**26**(2): 122-126
- [23] Lan KJ, Yen JY. Sliding mode control for active vibration isolation of a long range scanning tunneling microscope. *The Review of Scientific Instruments*. 2004;**75**(11):4367-4373
- [24] Kronmüller H, Goll D. Micromagnetic theory of the pinning of domain walls at phase boundaries. *Physica B*. 2002;**319**(1-4):122-126
- [25] Jiles DC, Atherton DL. Theory of ferromagnetic hysteresis (invited). *Journal of Applied Physics*. 1984;**55**(6): 2115-2120
- [26] Shu L, Chen DF, Lu QG. Modeling of time-delay in giant magnetostrictive actuator and Smith strategy. *Journal of System Simulation*. 2009;**21**(10): 3017-3021
- [27] Wang B, Cao S, Huang M. *Magnetostrictive Materials and Devices*. Beijing: Metallurgical Industry Press; 2008
- [28] Kim W j, Sadighi A. A novel low-power linear magnetostrictive actuator with local three-phase excitation. *IEEE/ASME Transactions on Mechatronics*. 2009;**21**(10):3017-3021
- [29] Young KD. A control engineer's guide to sliding mode control. *IEEE Transactions on Control Systems Technology*. 2004;**3**:156-164
- [30] Oliveiraa RCLF, de Oliveirab MC, Peresa PLD. Convergent LMI relaxations for robust analysis of uncertain linear systems using lifted polynomial parameter-dependent Lyapunov functions. *Systems & Control Letters*. 2008;**57**(8):680-668